JOURNAL OF GEOPHYSICAL RESEARCH, VOL. 114, B00A08, doi:10.1029/2008JB006038, 2009

Correlation of tremor activity with tidal stress in the northern Cascadia subduction zone

Anthony Lambert,[1] Honn Kao,[1] Garry Rogers,[1] and Nicholas Courtier[1]

Received 26 August 2008; revised 18 December 2008; accepted 22 May 2009; published 11 August 2009.

[1] We analyze hourly data from five tremor episodes in the northern Cascadia subduction zone over the period 2003–2005 provided by the Tremor Activity Monitoring System (TAMS). All five tremor episodes correspond to slow slip events observed by GPS. Fourier decomposition is used to separate the hourly tremor counts for each episode into "long-period" ($0 < f < 0.8$ cpd), "tidal" ($0.8 < f < 2.2$ cpd), and "short-period" ($f > 2.2$ cpd) components. The tidal component of the observations is compared with theoretical stress variations at depths of 20, 30, and 40 km, with 40 km being the depth of the interpreted subduction thrust interface. The stress variations are predicted by a 2-D ocean tide loading model combined with estimates of stress variations from Earth tides. We find that the shear stress in the thrust direction and the compressive normal stress on shallow dipping surfaces correlates with the data significantly better than the confining stress over the range of depths investigated. The relative amplitudes of tidal shear stress and compressive normal stress result in positive Coulomb stress favoring slip. Peak tremor activity occurs at times of maximum tidal shear stress in the thrust direction, which would assist slow slip and would suggest that tidal tremor and slip are colocated. The response of the tremor to tidal shear stress is roughly proportional to the mean activity level, controlled by tectonic conditions of stress and pore pressure. A significant, nontidal, daily variation in tremor activity of unknown origin is identified.

Citation: Lambert, A., H. Kao, G. Rogers, and N. Courtier (2009), Correlation of tremor activity with tidal stress in the northern Cascadia subduction zone, *J. Geophys. Res.*, *114*, B00A08, doi:10.1029/2008JB006038.

1. Introduction

[2] The discovery of nonvolcanic tremor associated with subduction in southwest Japan [*Obara*, 2002] and the recognition of the coincidence of tremor and slip in the Cascadia subduction zone and in the western Shikoku area, Japan [*Rogers and Dragert*, 2003; *Obara et al.*, 2004] has stimulated numerous investigations of the possible physical relationship between these two phenomena. In the northern Cascadia subduction zone the combined phenomenon, called episodic tremor and slip (ETS), exhibits an average recurrence interval beneath southern Vancouver Island of about 14.5±2 months coincident with transient slip along the deep portion of the interplate thrust zone just downdip of the locked zone [*Dragert et al.*, 2001; *Miller et al.*, 2002; *Wang et al.*, 2003]. In plan view the tremors occur in a band bounded approximately by the surface projections of the 30 and 50 km depth contours of the interpreted subduction thrust interface [*Flück et al.*, 1997] (Figure 1) and in cross section they occur over a depth interval of about 40 km with most tremors occurring in the continental crust [*Kao et al.*, 2005; *McCausland et al.*, 2005]. The horizontal migration of tremors during an episode in the northern Cascadia subduction zone is typically from southeast to northwest under Vancouver Island starting in central Puget Sound and moving with a relatively steady velocity interrupted from time to time by "halting and jumping" [*Kao et al.*, 2006, 2007a].

[3] Recently, it has been recognized that tremor in subduction zones is modulated by stress variations associated with Earth tides and ocean tide loading [*Nakata et al.*, 2006, 2007; *Rubinstein et al.*, 2008; *Shelly et al.*, 2007] and can be stimulated by the stress associated with surface waves (10–40 kPa) from large, distant earthquakes [*Miyazawa and Mori*, 2006; *Rubinstein et al.*, 2007; *Miyazawa and Brodsky*, 2008]. Nonvolcanic tremor can also be triggered in other tectonic environments other than subduction zones [*Gomberg et al.*, 2008]. In southwest Japan slow slip and tremor appear to be spatially and temporally coupled at or near the subduction thrust interface [*Obara et al.*, 2004; *Obara and Hirose*, 2006; *Shelly et al.*, 2006, 2007]. In contrast, tremor in northern Cascadia is found over a wider depth range, mostly above the interpreted subduction thrust interface, with temporally related slow slip occurring on the plate interface or possibly at a shallower depth [*Kao et al.*, 2005; *McCausland et al.*, 2005; *Wech and Creager*, 2007].

[4] The triggering of tremor by tidal stresses appears to require the additional influence of slow slip in subduction zones [cf. *Nakata et al.*, 2007], whereas the stresses associated with surface waves from large earthquakes seem to be large enough to trigger tremor independently of the local

[1]Geological Survey of Canada, Pacific Geoscience Centre, Sidney, British Columbia, Canada.

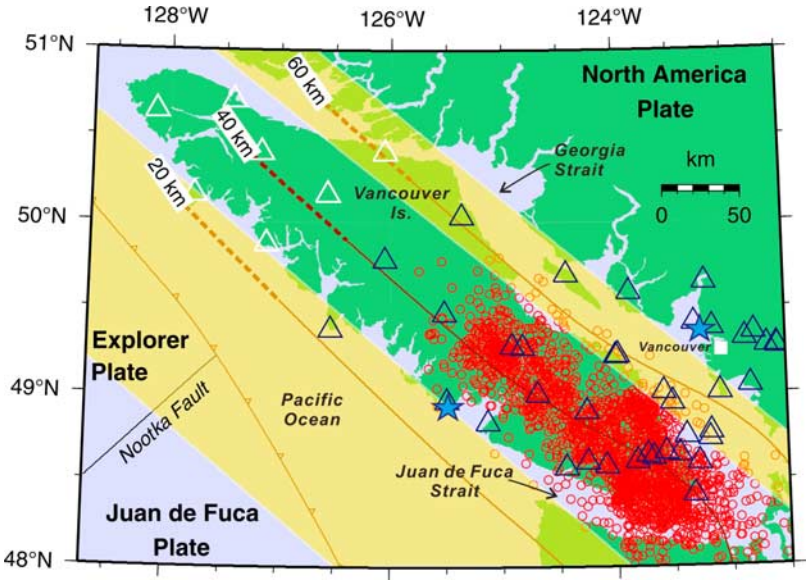

Figure 1. Location map showing the active area of tremor (red circles) under southern and central Vancouver Island over the period 2003–2005, the distribution of seismograph stations used in tremor monitoring (dark blue triangles), and the 2-D ocean tide loading approximation (yellow strips). Contours indicate interpreted depth to top of subducting Juan de Fuca Plate. Blue stars indicate the locations of the tidal reference stations at Point Atkinson (near Vancouver) and Ucluelet (on the Pacific coast).

tremor cycle [cf. *Rubinstein et al.*, 2007], although there is some evidence that the simultaneous occurrence of slow slip can enhance triggering even in the case of surface waves [*Miyazawa and Mori*, 2005]. This suggests that slow slip and tidal stress combine together to produce the physical conditions for the generation of tremor. It is not yet known whether the apparent lack of slow slip for minor tremor episodes in Cascadia [*McCausland et al.*, 2005] is simply a detection problem.

[5] In this paper five tremor episodes are analyzed over the period 2003 to 2005 to investigate the relationship between tremor activity and the different components of stress provided by ocean tide loading and Earth tides beneath Vancouver Island using a simple 2-D loading model (Figure 1). The objective is to determine which component of tidal stress is most effective in stimulating tremor and to examine how it might combine constructively with slow slip. To facilitate this analysis it was necessary to fit simultaneously a nontidal, solar daily variation in tremor activity.

2. Tremor Data Processing

[6] A continuous monitoring of tremor activity beneath Vancouver Island is provided by the Tremor Activity Monitoring System (TAMS) [*Kao et al.*, 2007b, 2008]. This system provides a count of the number of seismograph stations at which tremor waveforms are being recorded in any given 1-h period. The hourly counts are proportional to a combination of the tremor amplitude and the size of the active area. Over the study period (2003–2005) the number of stations in the TAMS network varies from 30 to 36 with a mean of 32. This variation is not expected to affect the counts associated with a typical tremor burst by more than one or two counts and is considered to have a negligible effect on this analysis. Moreover, the analysis method effectively normalizes the tidal response by a 4 day average of the tremor counts in each episode, which further reduces the effect of any small fluctuation in the number of seismograph stations.

[7] Using the TAMS data set over the period 2003–2005, five episodes of tremor activity were observed under southern and central Vancouver Island: (1) days 56–90, 2003; (2) days 329–365, 2003; (3) days 188–211, 2004; (4) days 323–341, 2004; and (5) days 243–274, 2005 (Figure 2). The criteria for selection of tremor episodes included the duration of the enhanced activity as well as the maximum daily count. Tremor episodes less than 1 week in duration were not considered in this study. Fourier decomposition was used to separate the tremor activity spectra, A(f), of each of these tremor episodes into three spectral components: A long-period component, L(f) ($0 < f < 0.8$ cpd), a "tidal" component, T(f) ($0.8 < f < 2.2$ cpd) and a short-period component, P(f) ($f > 2.2$ cpd) (See example, Figure 3). In the time domain the temporal variations in tremor activity, A(t), can be expressed in terms of (1) a long-period component, L(t), corresponding to the average activity level over slightly more than 1 day, (2) a tidal component, T(t), a combination of true tidal and other daily variations, and (3) a short-period component, P(t), incorporating pulses of activity lasting from 1 to 3 h. The mean count variance of 25.6 counts^2 for the five episodes studied is composed of 10.4 (long-period), 5.8 (tidal), and 9.4 (short-period). In this paper we analyze the nature and predictability of the tidal component of the five episodes of tremor activity.

3. Data Analysis Methodology

[8] Our analysis approach is to compare the temporal variations in tremor activity in the frequency band 0.8–2.2 cpd with estimates of different components of tidal

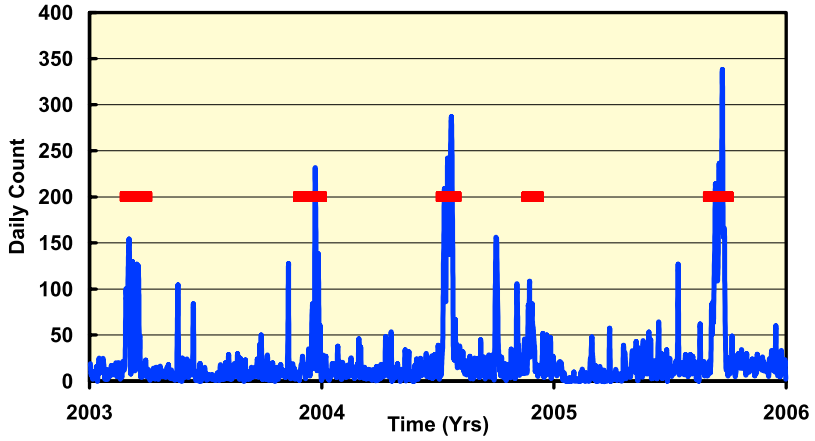

Figure 2. Temporal variation in tremor counts from the Tremor Activity Monitoring System (TAMS) on Vancouver Island. The time intervals over which tidal analyses were performed are indicated by horizontal red bars.

stress beneath southern Vancouver Island. We estimate ocean tide load stress, using an approximate 2-D loading model, as well as solid earth tide or body tide stress. A 2-D ocean tide loading model is reasonable as a first approximation when we consider that the ocean tide constituent phases in both the semidiurnal and diurnal bands change rather slowly over most of Georgia Strait and along the west coast of Vancouver Island [*Foreman et al.*, 1995; *Foreman and Thomson*, 1997]. The times of high and low water in each of these zones vary by significantly less than an hour. Moreover, in southern Juan de Fuca Strait, which is not included in the model, the semidiurnal tides exhibit an amphidrome (zero amplitude). We calculate tidal stresses relevant to the subduction zone interface beneath Vancouver Island, namely the stresses related to a plane at a depth of 40 km dipping at an angle of 15 degrees normal to the axis of the Island. Tidal stresses at shallower depths and the effect of increasing dip angle are also investigated. The stress components of interest are those that are expected to promote slip in the thrust sense or that would correlate with pore pressure variations, namely: the shear stress on the subduction interface in the thrust direction, the tensional stress normal to the interface that would reduce friction, and the mean confining stress (the negative of the mean tensional stress). In addition to the ocean tide load stresses, we calculate equivalent tidal stress components for the body tide acting directly on the Earth. The body tide stress components are estimated by calculating the body tide strains for a point on southern Vancouver Island and converting these to stresses using the stress-strain relations in spherical polar coordinates (details in section 4 and Appendix B).

[9] The influence of a particular tidal stress component on tremor activity is evaluated by least squares fitting the stress component as well as a nontidal solar daily component to the tidally filtered tremor activity data, over all five tremor episodes in the 2003–2005 period. A solar daily component is necessary to take into account an apparent daily variability in the TAMS data, which is either a real effect or a modulation of the TAMS detection threshold. The TAMS might be more sensitive at midnight than at noon when noise levels are generally higher. A similar nontidal daily variation in tremor amplitude was observed in the same area [*Rubinstein et al.*, 2008]. Owing to the similarity in

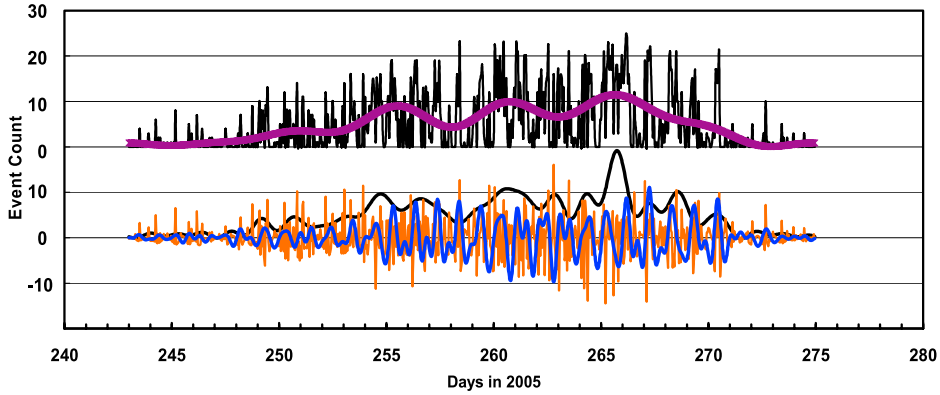

Figure 3. (top) Example of decomposition of tremor count series into (bottom) three spectral components: Long-period band (0–0.8 cpd; black curve), tidal band (0.8–2.2 cpd; blue curve) and short-period band (>2.2 cpd; orange curve). A long-period, tectonic envelope is defined by low-pass filtering the tremor count series with a cutoff at 0.25 cpd (purple curve; Figure 3, top).

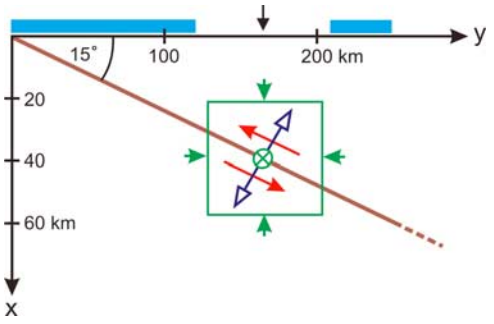

Figure 4. Cross section view of ocean tide, surface load configuration (horizontal blue bars) used in the plane strain computation, and stress components computed at the subduction interface beneath the center of Vancouver Island. The three stress components of interest are shear stress in the thrust direction (red arrows), tensional stress normal to the subduction interface (blue arrows), and 3-D confining stress (green arrows). The small green cross represents stress in the z direction (out of the page). The vertical scale is exaggerated by 2:1.

frequency of the solar daily variation and the diurnal tidal variation, the least squares fitting must include tremor episodes separated by at least 1 year.

4. Tidal Stress Modeling

4.1. Ocean Tide Load Stress

4.1.1. Computation Scheme

[10] We consider the loading of a semi-infinite, elastic half-space by two infinitely long strip loads representing the tides of Georgia Strait (width 40 km) and the tides on the Pacific Ocean coast (width 120 km), separated by Vancouver Island (width 90 km) (Figures 1 and 4). The computation scheme assumes plane strain, i.e., no along-axis (z) displacements but nonzero along-axis stress, with the y axis positive to the right and the x axis positive downward. We calculate the stress at different depths beneath central Vancouver Island arising from a meter of seawater in the two tidal regions by numerically integrating the effect of a line load on the surface. The required stress components are (1) the shear stress, τ_s, across planes parallel to the subduction interface, (2) the stress, σ_n, normal to such planes, and (3) the mean 3-D stress or dilatational stress (Σ) due to loading (Figure 4). Detailed expressions for the load stress components are given in Appendix A.

4.1.2. Ocean Tide Prediction Model

[11] The time-varying shear stress, normal stress and confining pressure at a given depth beneath the axis of Vancouver Island are computed by multiplying the stress components for a meter of seawater in each of the two zones by a corresponding tidal height prediction time series representative of each zone. For Georgia Strait we use tidal height predictions for Point Atkinson and for the Pacific Ocean coast we use predictions for Ucluelet (Figure 1). Tidal heights for the five tremor episodes were predicted using program Contide (S. Pagiatakis, personal communication, 2006) for the two representative ports using amplitudes and phase lags for the diurnal constituents K1, O1, P1, Q1, J1, M1 and the semidiurnal constituents M2, S2, N2, K2, NU2, MU2, L2, T2, 2N2 obtained from the Marine Environment Data Service, Fisheries and Oceans, Ottawa.

4.2. Body Tide Stress

[12] The body tide stresses for southern Vancouver Island were computed by predicting the time varying surface strains in spherical polar coordinates for a representative site and converting the strains to stresses. The tangential strains, $\varepsilon_{\theta\theta}$, $\varepsilon_{\varphi\varphi}$, $\varepsilon_{\theta\varphi}$ were predicted using subroutines NOMAN1 and NOMAN2 [*Harrison*, 1971] where θ is latitude north, φ is longitude east, positive $\varepsilon_{\theta\theta}$ and $\varepsilon_{\varphi\varphi}$ refers to extension and positive $\varepsilon_{\theta\varphi}$ refers to right-lateral shear. Love numbers h and l were taken to be 0.603 and 0.083, respectively, and radial variations in Love numbers are neglected in this treatment. (Note that since its publication, two errors in the strain part of NOMAN2 have been corrected: (1) an error in the sign of the deviatoric component of the L strain communicated by the author and (2) a factor of 2 in the semidiurnal, north-south component of the L strain, confirmed by A. K. Goodacre (personal communication, 2007).) Taking stresses in the crust to be approximately the same as at the Earth's surface, we have at the free surface $\sigma_{rr} = \sigma_{r\theta} = \sigma_{r\varphi} = 0$ and following from that $\varepsilon_{rr} = -[\nu/(1 - \nu)]\ [\varepsilon_{\theta\theta} + \varepsilon_{\varphi\varphi}]$ and $\varepsilon_{\theta r} = \varepsilon_{\varphi r} = 0$ [*Melchior*, 1978]. We calculate the full body tide stress tensor in spherical coordinates from the nonzero, independent components of the strain tensor, $\varepsilon_{\theta\theta}$, $\varepsilon_{\varphi\varphi}$, ε_{rr}, $\varepsilon_{\theta\varphi}$. Detailed expressions for the body tide stresses are given in Appendix B.

4.3. Computational Results

[13] We examine the theoretical ocean tide load stress variations near the subduction interface (40 km depth) and find that the ocean tide load shear stress exhibits the largest variation (peak-to-peak 4 kPa) followed by the load-related confining stress (peak-to-peak 3 kPa) and the load-related normal stress (peak-to-peak 2.5 kPa) (Figure 5). The load shear stress is also opposite in phase to the load normal stress (tension positive). The body tide stresses are relatively small compared to the load stresses, being 25%, 50%, and 10% as large as the load stresses for the shear stress, confining stress and normal stress, respectively (Figure 5). In addition, we observe that the load-related stresses are more semidiurnal in character than the body tide stress variations. For comparison with the observed tidal component of tremor activity we add the body tide stresses to the corresponding ocean tide load stresses to form the total shear stress, τ_{sT}, the total normal stress, σ_{nT}, and the total confining stress, Σ_T. Future investigations should employ a more detailed tidal loading representation around Vancouver Island and a 3-D stress computation that follows the day-to-day location of the tremors.

5. Data Analysis Results

[14] With reference to section 2 in which temporal variations in tremor activity, A(t), were expressed as A(t) = L(t) + T(t) + P(t) (e.g., Figure 3), we see that the tidal component exhibits a time-varying amplitude envelope. This suggests that the response to tidal forcing is modulated by the underlying tectonic condition associated with episodic tremor and slip. We find that a best fit tectonic

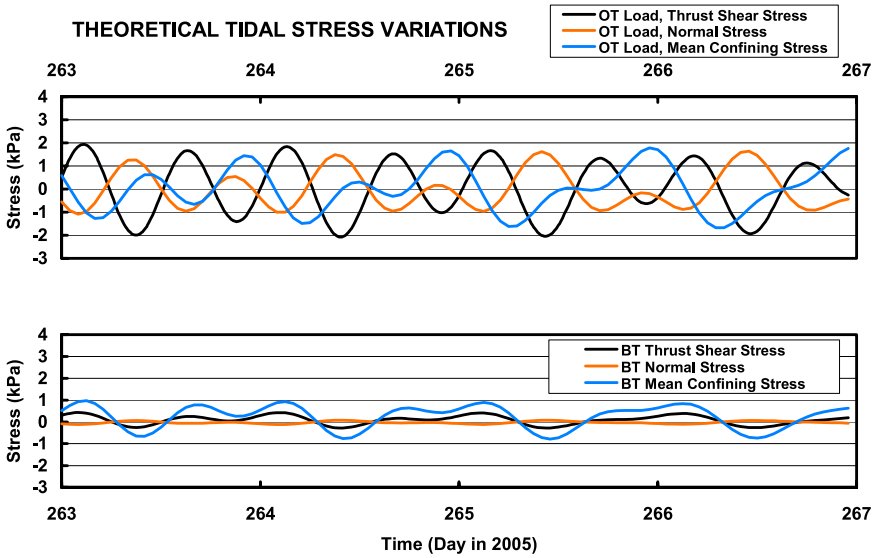

Figure 5. Theoretical tidal stress variations induced by (top) ocean tide loading and (bottom) the body tide at the subduction interface beneath Vancouver Island during the 2005 tremor episode.

envelope E(t) is obtained by further smoothing of the low-frequency component L(t) by a filter with a 0.25 cpd cutoff (Figure 3). In addition, the nontidal daily variation in the tremor count also appears to be linearly related to the long-term average tremor activity. Thus, a model for the 'tidal' variations in tremor activity, T(t), can be expressed in the form

$$T(t) = E(t)\,[k\sigma(t) + A\cos(2\pi\,t) + B\sin(2\pi\,t)] \qquad (1)$$

where $\sigma(t)$ represents the stress component or components most effective in driving the tidal variations in tremor activity, $A\cos(2\pi\,t) + B\sin(2\pi\,t)$ represents a nontidal daily variation in tremor activity, and k, A and B are constants to be determined.

[15] As described in section 3, we evaluate the influence of each of the three candidate stress components, $\sigma(t) = \tau_{sT}$, σ_{nT} and Σ_T, by fitting equation (1) by least squares simultaneously to all five tremor data sets over the 3 year period 2003–2005. Since the coherence between the tidal and nontidal input terms in equation (1) was found to be very low ($\gamma^2 = 0.003$) over the 3 year data set, the nontidal, solar daily term $A\cos(2\pi\,t) + B\sin(2\pi\,t)$ was first fitted to the data to produce a corrected data set against which the three stress models were evaluated. The nontidal daily variation was found to be highly significant, having an amplitude slightly larger than that of the tidal variation. Figure 6 shows the fitted nontidal terms for the three most active tremor episodes (episodes 1, 3, and 5; Figure 2). The phase lag of the daily variation is around 125°, which means that the maximum is just after midnight and the minimum is just after midday local time.

[16] We evaluate the three candidate tidal stress components by fitting them to the solar daily corrected, tremor activity data. The evaluation was carried out for depths of 20 km, 30 km and 40 km for a fault dip angle of 15° (Table 1) and for depths of 30 km and 40 km for a fault dip angle of 30° (Table 2). Results are given in terms of the fit parameter k and its standard error, an F statistic that expresses the probability that the variance of regression and the variance of the residual are drawn from a different population, and the % confidence that the stress parameter fits the data. F is defined as F = (ss(regression)/1)/(ss(residual)/(n − 1)), where ss refers to the sum of squares over all the data and n refers to the number of degrees of freedom of the residual, which is equal to the number of Fourier components in the tidal band minus two (coefficients A and B of the nontidal term).

[17] With reference to Table 1 the thrust shear stress and the normal stress for a 15° dip correlate well with the observed tidal component of the observed tremor for depths of 20–40 km, the correlation for shear stress being slightly greater. However, the sign of the correlation coefficient for the normal stress component corresponds to friction enhancement not friction reduction at times of higher tremor activity. The confining stress correlates relatively poorly with the observed tremor at all three depths compared to the thrust shear and normal stress but it is still significant. Figure 7 shows the solar daily corrected tremor activity data, the fitted tidal shear stress model at 40 km depth, and the residual for the three most active episodes. The residual data looks tidal as a result of being tidal band limited. Figure 8 compares the amplitude spectra of the tidal shear stress model at 40 km depth with the residuals for the same episodes. We see that the fit for episodes 3 (2004_1) and 5 (2005_1) is well above the noise whereas the fit for episode 1 (2003_1) is at noise level. All five episodes, fitted simultaneously, were required to obtain statistically significant results. The nontidal, solar daily term fitted alone reduced the overall tidal band variance from 5.7 to 3.5 counts^2, the tidal model alone reduces the tidal band variance from 5.7 to 4.5 counts^2, and the two together reduce the tidal band variance to 2.5 counts^2.

[18] With reference to Table 2 the thrust shear stress and normal stress for a 30° dip show a reduced correlation with the tremor data, the normal stress correlating slightly better than the shear stress. Moreover, smaller scaling parameters,

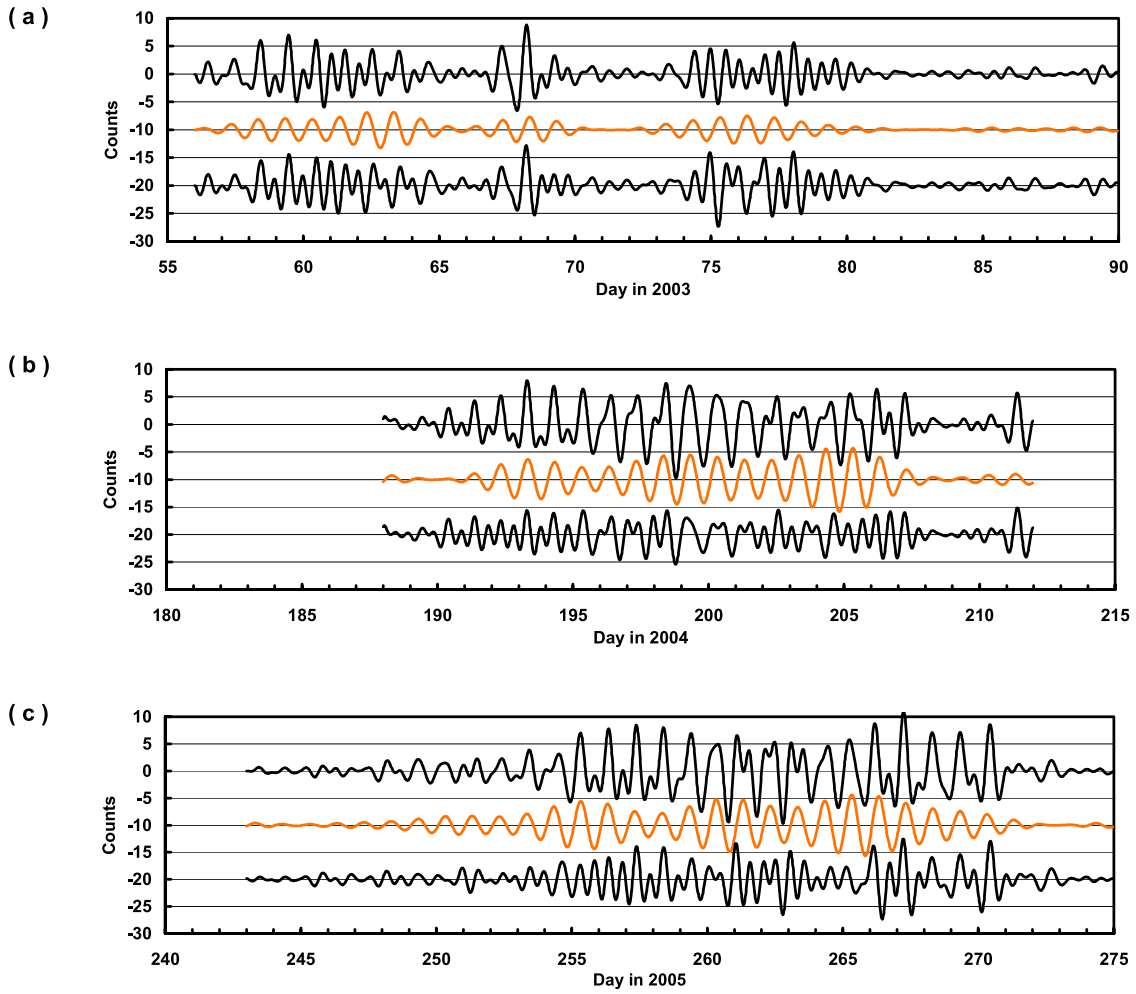

Figure 6. Examples of the tidal band tremor activity data (top black curves), the fitted nontidal, solar daily variation (orange curves) and the corrected tidal band data (bottom black curves) for the three most active tremor episodes, (a) 2003_1, (b) 2004_1, and (c) 2005_1.

k, for normal stress indicate that the normal stress is larger than the shear stress when the dip of the surface is greater, leading to smaller or negative Coulomb stress. Thus, faults parallel to the interpreted subduction interface with a dip of 15° are more likely to be activated by tidal stress than more steeply dipping surfaces.

6. Discussion

[19] Our results show clearly that tremor activity beneath Vancouver Island responds to variations in both tidal shear and normal stress, the shear stress having the greater amplitude. The identification of ocean load shear stress as the driver of the tidal variations in tremor activity is facilitated by the fact that the character of the load-induced shear stress beneath Vancouver Island is significantly different from the character of the load-induced confining stress (Figure 5). The shear stress has a much stronger semidiurnal character than the confining stress for the following reasons: (1) a surface load downdip of the computation point (Georgia Strait) produces shear in the thrust direction, whereas a surface load updip of the computation point (Pacific Ocean coast) produces shear in the normal direction, (2) both downdip and updip surface loads contribute positively to confining stress, and (3) the semidiurnal tides in Georgia Strait are virtually 180° out of phase with the semidiurnal tides on the Pacific Ocean coast, whereas the diurnal phase difference across the Island is

Table 1. Results of Multiple Linear Regression of Tidal Band Tremor Activity With Three Different Tidal Stress Components at Depths of 40, 30, and 20 km for a Slip Surface Dip of 15°[a]

Depth (km)	Fit Parameter	Thrust Shear Stress	Normal Stress	Confining Stress
40	k	0.170	−0.204	−0.066
	SE (k)	0.004	0.006	0.005
	F	170.5	129.4	19.3
	Conf	93.9%	93.0%	82.0%
30	k	0.210	−0.304	−0.082
	SE (k)	0.006	0.009	0.005
	F	170.5	141.3	24.5
	Conf	93.9%	93.3%	84.0%
20	k	0.291	−0.583	−0.111
	SE (k)	0.008	0.016	0.006
	F	155.8	150.2	32.1
	Conf	93.6%	93.5%	86.0%

[a]Tremor activity has previously been corrected for a solar daily variation. SE, standard error; units of k and SE(k) are kPa^{-1}. For definition of F, see text.

Table 2. Results of Multiple Linear Regression of Tidal Band Tremor Activity With Three Different Tidal Stress Components at Depths of 40 and 30 km for a Slip Surface Dip of 30°[a]

Depth (km)	Fit Parameter	Thrust Shear Stress	Normal Stress	Confining Stress
40	k	0.202	−0.132	−0.066
	SE (k)	0.007	0.004	0.005
	F	104.1	111.9	19.3
	Conf	92.2%	92.4%	82.0%
30	k	0.192	−0.168	−0.082
	SE (k)	0.007	0.006	0.005
	F	85.9	110.2	24.5
	Conf	91.4%	92.4%	84.0%

[a]Tremor activity has previously been corrected for a solar daily variation.

only about 45°. Thus, semidiurnal ocean tide loads on the opposite sides of the Island add for shear stress and subtract for confining stress providing a useful difference in character.

[20] The analysis results given in Table 1 show that the band-limited tremor activity is correlated with both the tidal shear stress in the thrust direction and the tidal normal stress at the depth of the interpreted subduction thrust interface. The correlation coefficient for the normal stress is negative, however, which means that when the shear stress is maximum, so is the friction. Nevertheless, the Coulomb stress that would promote shear failure, $\tau_{sT} + \mu\,\sigma_{nT}$, where μ is the friction coefficient, is positive, since τ_{sT} is larger than σ_{nT}, σ_{nT} is negative and μ is generally taken to be around 0.4 (A lower or a variable value may be appropriate for slow slip). We estimate a peak-to-peak Coulomb stress variation of at least 3 kPa. Thus, the shear stress provided by ocean tide loading and partly by Earth tides is clearly able to promote slip at the (40 km) depth of the interpreted subduction thrust interface. The changing value of the scaling coefficient k with depth indicates that the tidal shear stress decreases at shallower depths but so does the negative normal stress, so that the Coulomb stress decreases only slightly between 40 and 20 km. Thus, the Coulomb stress conditions would promote shear failure over a range of depths in the crust above the interface, including at a depth of 30 km, the mean depth of the tremors beneath Vancouver Island, and the location of the bottom of the E reflectors [*Clowes et al.*, 1987]. Moreover, shallow dipping structures would be more favorably activated by tidal stress than steeper structures.

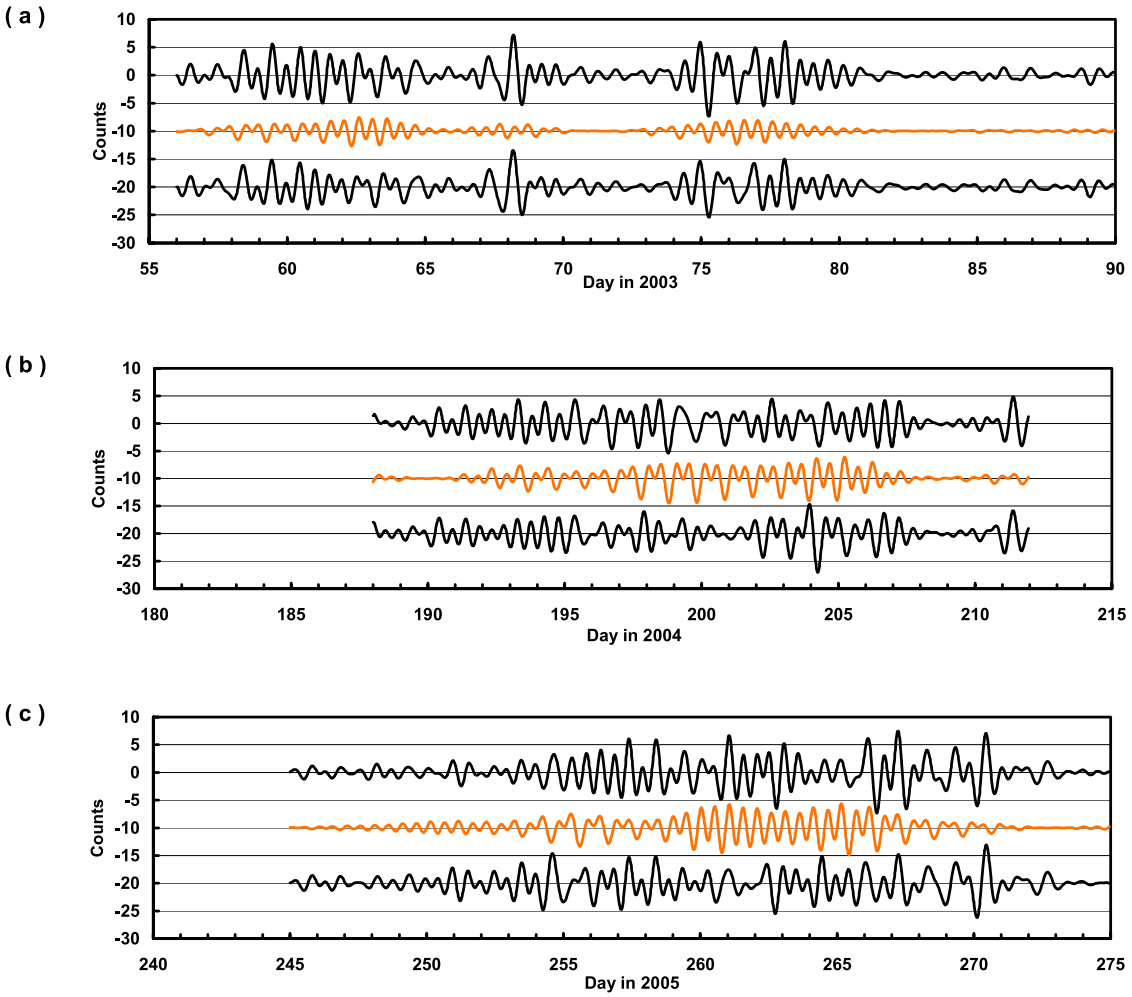

Figure 7. Examples of the solar daily corrected tremor activity data (top black curves), the fitted tidal shear stress model at 40 km depth (orange curves), and the residual (bottom black curves) for the three most active episodes, (a) 2003_1, (b) 2004_1, and (c) 2005_1.

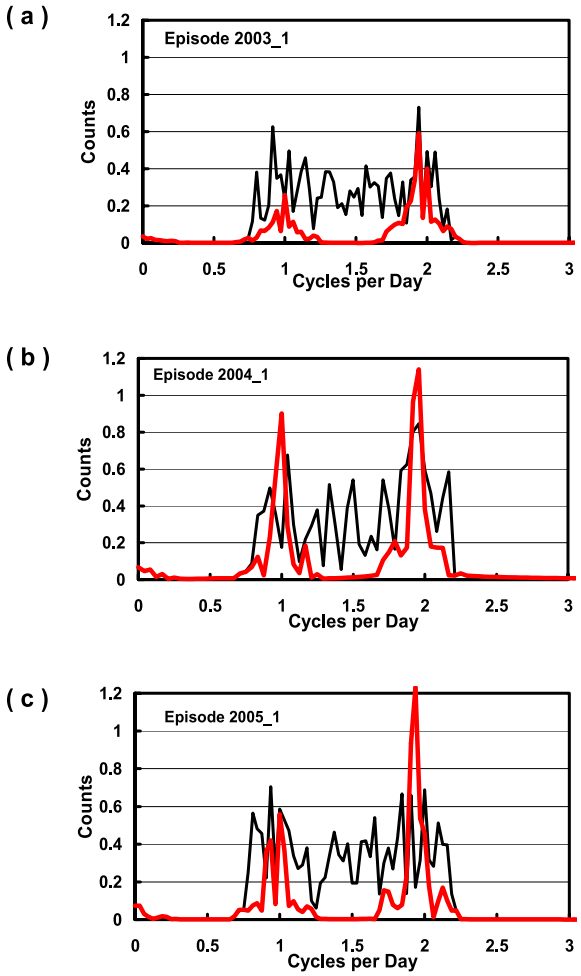

Figure 8. Amplitude spectra for the fitted tidal shear stress model (red curves) and the residual tidal band data (black curves) for the three episodes, (a) 2003_1, (b) 2004_1, and (c) 2005_1, shown in Figure 7.

[21] An important fact to note is that all five tremor episodes analyzed here correspond to slow slip. Episodes 1, 3, and 5 begin beneath the Olympic peninsula of Washington State and move north under southern Vancouver Island, corresponding to eastward movements of about 5 mm measured by GPS on southern Vancouver Island (GPS station ALBH relative to DRAO) [*Rogers and Dragert*, 2003]. Episode 2 began on northern Vancouver Island and moved south to central Vancouver Island, dying out before reaching the south end of the Island. Episode 4 was confined to central Vancouver Island. Both of these last two episodes corresponded to motion reversals observed at GPS station Ucluelet (UCLU) (H. Dragert, personal communication, 2008). A similar association between tidal tremor and slip is found in Japan [cf. *Nakata et al.*, 2007].

[22] The observed positive correlation between tidal tremor and tidal shear stress that would facilitate slip in the thrust direction on shallow dipping surfaces suggests that slip and tremor are directly related. The lower correlation between tidal confining stress and tremor activity diminishes the possibility that tidal tremor is a response to pore pressure variations. Moreover, our finding that tidal stress would enhance slip at depths shallower than the originally interpreted subduction thrust would support the idea that tidally varying tremor and slip are colocated and distributed over a range of depths (compare model B of *Kao et al.* [2006]). S wave polarization of tremor is also consistent with slip being on faults parallel to the subduction thrust interface, and the collocation of slip and tremor over a range of depths cannot be ruled out [*Wech and Creager*, 2007]. If we agree that tremor and slip are colocated, the analysis results suggest that tremor only occurs during slip in the thrust direction and not in the normal or back slip direction. Otherwise, the tremor activity would look like a rectified version of the tidal shear stress. This could mean either that there is no slip in the normal or back slip direction, or that the back slip is silent. Possibly the combination of increasing thrust shear stress and compressive normal stress, which would occur during positive peaks, is required to produce tremor on low-friction surfaces. The possibility that slip could reverse direction under the influence of tidal loading is supported by the fact that change in shear stress over a tidal cycle is a significant fraction of the cumulative stress drop associated with a typical slow slip episode. Modeling of the effect of slow slip on stress conditions surrounding the slip zone predicts a total cumulative stress drop in thrust-positive Coulomb stress of around 10 kPa [*Dragert et al.*, 2004] compared to a twice daily tidal Coulomb stress variation of around 3 kPa. Thus, it is important to investigate the nature of the slow slip response to tidal forcing. A distorted tidal strain signature might be expected at the surface, if tidal shear produces slip in only the thrust direction. Tidally varying slip has not yet been observed in northern Cascadia, nor elsewhere in the world.

[23] There is ample evidence for cumulative shear over geological time collocated with high fluid pore pressure beneath Vancouver Island. Such a distributed shear zone would correspond to the location of the E reflectors dipping parallel to the deeper postulated subduction thrust interface. The E reflectors have been identified as a zone of underplating [*Clowes et al.*, 1987], a zone of high electrical conductivity and fluid pore pressure [*Hyndman*, 1988], a low-velocity zone [*Cassidy and Ellis*, 1993], and a zone of shear deformation [*Calvert and Clowes*, 1990; *Nedimović et al.*, 2003] and subducted oceanic crust [*Nicholson et al.*, 2005]. *Nedimović et al.* [2003] note that the E reflection zone appears to be aseismic and speculate that the E layer may, in fact, be the site of slow slip.

[24] The response to tidal shear stress typically varies through a tremor episode, increasing from near zero to a finite level before diminishing back to zero at the end of the episode (Figure 3). The trigger for the ETS event is clearly not the tides. We speculate that a combination of stress accumulation and pore pressure buildup initiates slow slip. As slip begins the friction coefficient drops to a lower value allowing tidal action to increase over a period of a few days to a constant level until accumulated stress and pore pressure are dissipated. A central feature of our empirical model (equation (1)) is the adoption of the long-term average tremor activity as a proxy for the unknown, nontidal, parameter controlling strength and friction conditions on one or more slow slip interfaces. Despite the

evidence for distributed slip assisted by the tides, the high-frequency, pulse-like component of tremor remains unexplained. These very significant variations are suggestive of slip associated with elevated pore pressure relieved through fluid flow. Individual fault segments may slip until generally elevated pore pressures are relieved through fluid flow, while others slip at the times of peak tidal shear stress.

[25] The presence of a nontidal, diurnal signal in the tremor amplitudes beneath the northern Cascadia subduction zone has already been noted by *Rubinstein et al.* [2008]. Nevertheless, the large amplitude of the nontidal, daily variation in tremor activity, slightly larger than the tidal variation (Figures 6 and 7), is an unexpected outcome of our analysis. One possibility is that the TAMS detection threshold is modulated by cultural and wind noise, the detection threshold being highest (least sensitive) just after noon and lowest (most sensitive) just after midnight. However, if this were true, the daily variation would modulate the observed tidal variation, giving rise to certain characteristic sum and difference frequencies. These frequencies have not been detected in the tremor activity data. The origin of the nontidal daily variation remains unknown.

7. Conclusion

[26] Tremor activity during five consecutive ETS events beneath southern and central Vancouver Island correlates significantly better with tidal shear stress and compressive normal stress on shallow dipping surfaces than with tidal confining stress. The relative amplitudes of tidal shear stress and compressive normal stress result in positive Coulomb stress favoring slip. Peak tremor activity occurs at times of maximum tidal shear stress in the thrust direction, which would assist slow slip and would suggest that tidal tremor and slip are colocated. Tidal stress is capable of assisting both slow slip and tremor over a range of depths from 20 to 40 km. The response of the tremor to tidal shear stress is roughly proportional to the mean activity level, controlled by tectonic conditions of stress and pore pressure. A significant, nontidal, daily variation in tremor activity of unknown origin is identified. Its amplitude is slightly larger than that of the tidal variations.

Appendix A: Load Stress at Depth Using a 2-D Plane Strain Model

[27] With reference to Figure 4, the stresses in Cartesian coordinates at a point x,y produced by a line load of width dw at x = 0, y = 0 can be expressed as

$$\begin{aligned} d\sigma_{xx} = -2P(dw)x^3/\pi\, r^4, d\sigma_{yy} = -2P(dw)xy^2/\pi\, r^4, d\tau_{xy} \\ = -2(dw)Px^2\, y/\pi\, r^4 \end{aligned} \quad \text{(A1)}$$

where P is the load pressure, r is the radial distance to the computation point in the medium, and positive stress is defined to be tension [e.g., *Jaeger*, 1962]. The line load stresses are numerically integrated to give the total load stresses at depth x, σ_{xx} (x), σ_{yy} (x), τ_{xy} (x), resulting from 1 m of seawater in each of the two tidal zones. These stresses are then resolved into stress components relevant to the dynamics of the subduction interface beneath central Vancouver Island (Figure 4). Expressed in terms of the Cartesian total load stresses derived from (A1), we have

$$\begin{aligned} \tau_s(x) &= \left[\sigma_{yy}\,(x) - \sigma_{xx}\,(x)\right]\sin\delta\cos\delta - \tau_{xy}(x) \\ &\quad \cdot (\cos\delta\cos\delta - \sin\delta\sin\delta) \\ \sigma_n(x) &= \sigma_{xx}(x)\cos^2\delta + \sigma_{yy}(x)\sin^2\delta - 2\,\tau_{xy}\,(x)\sin\delta\cos\delta \\ \Sigma(x) &= \left[\sigma_{xx}(x) + \sigma_{yy}(x) + \sigma_{zz}(x)\right]/3 \end{aligned} \quad \text{(A2)}$$

where $\sigma_{zz} = \nu\,(\sigma_{xx}\,(x) + \sigma_{yy}\,(x))$, δ is the dip angle of the subduction interface, and ν is Poisson's ratio taken here as 0.28. Positive τ_s corresponds to "normal" shear stress, and positive σ_n and Σ correspond to tension.

Appendix B: Body Tide Stress From Body Tide Strain

[28] We calculate the body tide stress tensor from the nonzero, independent components of strain using the generalized form of Hooke's law [e.g., *Ranalli*, 1995]

$$\sigma = \lambda\,(\nabla \cong u)\,I + 2\mu\varepsilon \quad \text{(B1)}$$

where σ is the stress tensor, $\nabla \cong u$ is the divergence of the displacement vector u, I is the unit matrix, ε is the strain tensor, and λ and μ are the Lamé's parameters. Using (B1) and recognizing that $\nabla \cong u = \varepsilon_{rr} + \varepsilon_{\theta\theta} + \varepsilon_{\varphi\varphi}$ in spherical polar coordinates, the nonzero spherical polar stress components can be expressed as

$$\begin{aligned} \sigma_{\theta\theta} &= \lambda\left(\varepsilon_{rr} + \varepsilon_{\theta\theta} + \varepsilon_{\varphi\varphi}\right) + 2\mu\,\varepsilon_{\theta\theta} \\ \sigma_{\varphi\varphi} &= \lambda\left(\varepsilon_{rr} + \varepsilon_{\theta\theta} + \varepsilon_{\varphi\varphi}\right) + 2\mu\,\varepsilon_{\varphi\varphi} \\ \sigma_{\theta\varphi} &= \mu\varepsilon_{\theta\varphi} \end{aligned} \quad \text{(B2)}$$

where $\lambda = 3.42 \times 10^{10}$ Pa and $\mu = 2.66 \times 10^{10}$ Pa. The tangential body tide stress at an azimuth α is given by

$$\sigma_\alpha = \sigma_{\theta\theta}\cos^2\alpha + \sigma_{\varphi\varphi}\sin^2\alpha + 2\sigma_{\theta\varphi}\sin\alpha\cos\alpha \quad \text{(B3)}$$

[29] Thus, the tangential stresses normal and parallel to the axis of Vancouver Island (azimuths 45° and 315°) are

$$\begin{aligned} \sigma_{45} &= \sigma_{\theta\theta}/2 + \sigma_{\varphi\varphi}/2 + \sigma_{\theta\varphi} \\ \sigma_{315} &= \sigma_{\theta\theta}/2 + \sigma_{\varphi\varphi}/2 - \sigma_{\theta\varphi} \end{aligned}$$

Expressing the body tide stresses in terms of the Cartesian coordinate system employed in the computation of ocean load stresses (section 4.1.1, Figure 4), we have

$$\sigma_{xx}(x) = 0, \sigma_{yy}(x) = \sigma_{45}, \sigma_{zz}(x) = \sigma_{315} \text{ and } \tau_{xy}(x) = 0 \quad \text{(B4)}$$

Therefore, the time varying stresses for the body tide equivalent to those for the load tide (A2) are approximately constant for all depths, x, in the crust and are given by

$$\begin{aligned} \tau_s &= \sigma_{45}\sin\delta\cos\delta \\ \sigma_n &= \sigma_{45}\sin^2\delta \\ \Sigma &= (\sigma_{45} + \sigma_{315})/3 \end{aligned} \quad \text{(B5)}$$

where δ is the dip angle of the subduction interface.

[30] **Acknowledgments.** We thank Tom James and Alan Goodacre for assistance with prediction of Earth tide stress and Herb Dragert and Kelin Wang for useful discussions on slow slip and subduction zone dynamics. We thank Duncan Agnew and John Vidale and the Associate Editor for suggesting improvements to the manuscript. Geological Survey of Canada contribution 20080352.

References

Calvert, A. J., and R. M. Clowes (1990), Deep, high-amplitude reflections from a major shear zone above the subducting Juan de Fuca plate, *Geology*, *18*, 1091–1094, doi:10.1130/0091-7613(1990)018<1091:DHARFA>2.3.CO;2.

Cassidy, J. F., and R. M. Ellis (1993), S wave velocity structure of the northern Cascadia subduction zone, *J. Geophys. Res.*, *98*, 4407–4421, doi:10.1029/92JB02696.

Clowes, R. M., M. T. Brandon, A. G. Green, C. J. Yorath, A. S. Brown, E. R. Kanasewich, and C. Spencer (1987), LITHOPROBE-southern Vancouver Island: Cenozoic subduction complex imaged by deep seismic reflections, *Can. J. Earth Sci.*, *24*, 31–51.

Dragert, H., K. Wang, and T. S. James (2001), A silent slip event on the deeper Cascadia subduction interface, *Science*, *292*, 1525–1528, doi:10.1126/science.1060152.

Dragert, H., K. Wang, and G. Rogers (2004), Geodetic and seismic signatures of episodic tremor and slip in the northern Cascadia subduction zone, *Earth Planets Space*, *56*, 1143–1150.

Flück, P., R. D. Hyndman, and K. Wang (1997), Three-dimensional dislocation model for great earthquakes of the Cascadia subduction zone, *J. Geophys. Res.*, *102*, 20,539–20,550, doi:10.1029/97JB01642.

Foreman, M. G. G., and R. E. Thomson (1997), Three-dimensional model simulations of tides and buoyancy currents along the west coast of Vancouver Island, *J. Phys. Oceanogr.*, *27*, 1300–1325, doi:10.1175/1520-0485(1997)027<1300:TDMSOT>2.0.CO;2.

Foreman, M. G. G., R. A. Walters, R. F. Henry, C. P. Keller, and A. G. Dolling (1995), A tidal model for eastern Juan de Fuca Strait and the southern Strait of Georgia, *J. Geophys. Res.*, *100*, 721–740, doi:10.1029/94JC02721.

Gomberg, J., J. L. Rubinstein, Z. Peng, K. C. Creager, J. E. Vidale, and P. Bodin (2008), Widespread triggering of nonvolcanic tremor in California, *Science*, *319*, 173, doi:10.1126/science.1149164.

Harrison, J. C. (1971), New computer programs for the calculation of Earth tides, 29 pp., Co-op. Inst. for Res. in Environ. Sci., Univ. of Colo., Boulder.

Hyndman, R. D. (1988), Dipping seismic reflectors, electrically conductive zones, and trapped water in the crust over a subducting plate, *J. Geophys. Res.*, *93*, 13,391–13,405, doi:10.1029/JB093iB11p13391.

Jaeger, J. C. (1962), *Elasticity, Fracture and Flow with Engineering and Geological Applications*, Methuen, London.

Kao, H., S.-J. Shan, H. Dragert, G. Rogers, J. F. Cassidy, and K. Ramachandran (2005), A wide depth distribution of seismic tremors along the northern Cascadia margin, *Nature*, *436*, 841–844, doi:10.1038/nature03903.

Kao, H., S.-J. Shan, H. Dragert, G. Rogers, J. F. Cassidy, K. Wang, T. S. James, and K. Ramachandran (2006), Spatial-temporal patterns of seismic tremors in northern Cascadia, *J. Geophys. Res.*, *111*, B03309, doi:10.1029/2005JB003727.

Kao, H., S.-J. Shan, G. Rogers, and H. Dragert (2007a), Migration characteristics of seismic tremors in the northern Cascadia margin, *Geophys. Res. Lett.*, *34*, L03304, doi:10.1029/2006GL028430.

Kao, H., P. J. Thompson, G. Rogers, H. Dragert, and G. Spence (2007b), Automatic detection and characterization of seismic tremors in northern Cascadia, *Geophys. Res. Lett.*, *34*, L16313, doi:10.1029/2007GL030822.

Kao, H., P. J. Thompson, S.-J. Shan, G. Rogers, H. Dragert, and G. Spence (2008), Tremor Activity Monitoring in northern Cascadia, *Eos Trans. AGU*, *89*(42), 405–406, doi:10.1029/2008EO420001.

McCausland, W., S. Malone, and D. Johnson (2005), Temporal and spatial occurrence of deep non-volcanic tremor: From Washington to northern California, *Geophys. Res. Lett.*, *32*, L24311, doi:10.1029/2005GL024349.

Melchior, P. (1978), *The Tides of the Planet Earth*, Pergamon, Oxford, U. K.

Miller, M. M., T. Melbourne, D. J. Johnson, and W. Q. Sumner (2002), Periodic slow earthquakes from the Cascadia subduction zone, *Science*, *295*, 2423, doi:10.1126/science.1071193.

Miyazawa, M., and E. E. Brodsky (2008), Deep low-frequency tremor that correlates with passing surface waves, *J. Geophys. Res.*, *113*, B01307, doi:10.1029/2006JB004890.

Miyazawa, M., and J. Mori (2005), Detection of triggered deep low frequency events from the 2003 Tokachi-oki earthquake, *Geophys. Res. Lett.*, *32*, L10307, doi:10.1029/2005GL022539.

Miyazawa, M., and J. Mori (2006), Evidence suggesting fluid flow beneath Japan due to periodic seismic triggering from the 2004 Sumatra-Andaman earthquake, *Geophys. Res. Lett.*, *33*, L05303, doi:10.1029/2005GL025087.

Nakata, R., N. Suda, and H. Tsuruoka (2006), Tidal synchronicity of the low-frequency tremor in eastern Shikoku, Japan, *Eos Trans. AGU*, *87*(52), Fall Meet. Suppl., Abstract V41A-1700.

Nakata, R., N. Suda, and H. Tsuruoka (2007), Occurrence of deep low-frequency tremors synchronized to Earth tides, *Eos Trans. AGU*, *88*(52), Fall Meet. Suppl., Abstract T12C-05.

Nedimović, M. R., R. D. Hyndman, K. Ramachandran, and G. D. Spence (2003), Reflection signature of seismic and aseismic slip on the northern Cascadia subduction interface, *Nature*, *424*, 416–420, doi:10.1038/nature01840.

Nicholson, T., M. Bostock, and J. F. Cassidy (2005), New constraints on subduction zone structure in northern Cascadia, *Geophys. J. Int.*, *161*, 849–859, doi:10.1111/j.1365-246X.2005.02605.x.

Obara, K. (2002), Nonvolcanic deep tremor associated with subduction in southwest Japan, *Science*, *296*, 1679–1681, doi:10.1126/science.1070378.

Obara, K., and H. Hirose (2006), Non-volcanic deep low-frequency tremors accompanying slow slips in the south west Japan subduction zone, *Tectonophysics*, *417*, 33–51, doi:10.1016/j.tecto.2005.04.013.

Obara, K., H. Hirose, F. Yamamizu, and K. Kasahara (2004), Episodic slow slip events accompanied by non-volcanic tremors in southwest Japan subduction zone, *Geophys. Res. Lett.*, *31*, L23602, doi:10.1029/2004GL020848.

Ranalli, G. (1995), *Rheology of the Earth*, 2nd ed., Chapman and Hall, London.

Rogers, G., and H. Dragert (2003), Episodic tremor and slip on the Cascadia subduction zone: The chatter of silent slip, *Science*, *300*, 1942–1943, doi:10.1126/science.1084783.

Rubinstein, J. L., J. E. Vidale, J. Gomberg, P. Bodin, K. C. Creager, and S. D. Malone (2007), Non-volcanic tremor driven by large transient shear stresses, *Nature*, *448*, 579–582, doi:10.1038/nature06017.

Rubinstein, J. L., M. La Rocca, J. E. Vidale, K. C. Creager, and A. G. Wech (2008), Tidal modulation of nonvolcanic tremor, *Science*, *319*, 186–189, doi:10.1126/science.1150558.

Shelly, D. R., G. C. Beroza, S. Ide, and S. Nakamula (2006), Low frequency earthquakes in Shikoku, Japan, and their relationship to episodic tremor and slip, *Nature*, *442*, 188–191, doi:10.1038/nature04931.

Shelly, D. R., G. C. Beroza, and S. Ide (2007), Complex evolution of transient slip derived from precise tremor locations in western Shikoku, Japan, *Geochem. Geophys. Geosyst.*, *8*, Q10014, doi:10.1029/2007GC001640.

Wang, K., R. Wells, S. Mazzotti, R. D. Hyndman, and T. Sagiya (2003), A revised dislocation model of interseismic deformation of the Cascadia subduction zone, *J. Geophys. Res.*, *108*(B1), 2026, doi:10.1029/2001JB001227.

Wech, A. G., and K. C. Creager (2007), Cascadia tremor polarization evidence for plate interface slip, *Geophys. Res. Lett.*, *34*, L22306, doi:10.1029/2007GL031167.

N. Courtier, H. Kao, A. Lambert, and G. Rogers, Geological Survey of Canada, Pacific Geoscience Centre, 9860 West Saanich Road, Sidney, BC V8L 4B2, Canada. (tlambert@nrcan.gc.ca)